

Comparing Simulation and Experiment of a 2D Granular Couette Shear Device

Marc Lätzel, Stefan Luding* and Hans J. Herrmann

Institute for Computer Applications 1, Pfaffenwaldring 27, 70569 Stuttgart, Germany

Daniel W. Howell and R. P. Behringer

*Department of Physics and Center for Nonlinear and Complex Systems,
Duke University, Durham NC, 27708-0305, USA*

(Dated: March 29, 2005)

We present experiments along with molecular dynamics (MD) simulations of a two-dimensional (2D) granular material in a Couette cell undergoing slow shearing. The grains are disks confined between an inner, rotating wheel and a fixed outer ring. The simulation results are compared to experimental studies and quantitative agreement is found. Tracking the positions and orientations of individual particles allows us to obtain density distributions, velocity and particle rotation rate for the system. The key issue of this paper is to show the extent to which *quantitative* agreement between an experiment and MD simulations is possible. Besides many differences in model-details and the experiment, the qualitative features are nicely reproduced. We discuss the quantitative agreement/disagreement, give possible reasons, and outline further research perspectives.

I. INTRODUCTION

The pioneering work of Reynolds in 1885 [1] and the more elaborate investigations by Bagnold [2] were among the first experiments to closely address the problem of granular shearing. Recently the subject of granular shearing has regained much interest in the physics community due to the appearance of this process in common granular flows such as convection [3], pipe and chute flow [4, 5], avalanches [6, 7], crack formation, and earthquakes [8].

In the traditional picture for shearing of a dense granular material, grains are assumed to be relatively hard so that they maintain their volume and shape under applied forces. If shear is applied to a granular sample, in principle, the grains will respond elastically (i.e. reversibly) up to the point of failure. The response in the elastic regime is still an open question which is not addressed here [9, 10, 11] because we focus on the regime of extended deformation. Under shear, the grains will dilate against a normal load, up to the point of failure. Under continued shearing the system appears to approach a steady state, that is typically characterized by localized failure in narrow regions known as shear bands. An extremely slow compaction/rearrangement can also occur under steady shearing [12]. However, this effect will be disregarded in the following. Here we are more concerned with the kinematics of the particles in the “quasi steady state”.

Recent experiments on granular shearing have primarily focused on the force properties of the system [12, 13, 14, 15, 16, 17]. Only a few experiments have explored the kinematics of shear zones, and these involved using either inclined or vertical chutes [4, 5, 18]

or vibrated beds [19] where air flow between the particles may also have been important. In a single case of which we are aware, Buggisch and Löffelmann [20] investigated the mixing mechanisms due to shearing in a 2D annular cell similar to the one described here. This experiment involved flexible boundaries, in contrast to the fixed volume used in our work.

The simulations presented in this study are perhaps unique in that they 1) match with considerable fidelity the parameters in a set of experiments, and 2) the simulations and experiments yield detailed properties which can be mutually compared. Thus, the goals of this work include the deepening of insight into an important granular system, and the opportunity to explore how well a class of models captures experimental observations. The relevance of this latter issue is underscored by a recent study in which diverse groups modeling flow in a hopper, obtained an equally diverse set of predictions, many of which did not match experiment [21, 22, 23].

In our experiment a 2D Couette cell filled with photoelastic polymer disks is used to study both the mean and statistical properties of the flow. Using particle tracking techniques, the spin and transport velocity profiles as well as the associated density variations during steady state shearing can be measured. Because the particles are photoelastic, it is also possible to infer information on the local stress state of the system, a topic which is considered elsewhere [11].

The following are the key observations from these studies: A short time after the beginning of shearing, a shear zone forms near the inner wall. The location of the shear band close to the inner wall can be attributed to the fact that the shear stress is highest there (decaying proportional to $(r - R)^{-2}$), as was observed from previous simulations [24, 25] and as is consistent with the static equilibrium conditions of continuum theory in cylindrical coordinates. The characteristic width of the induced shear band is found to be a few particle diameters, almost independent of the average packing fraction. The

*new address: Particle Technology, DelftChemTech, TU Delft, Julianalaan 136, 2628 BL Delft, The Netherlands

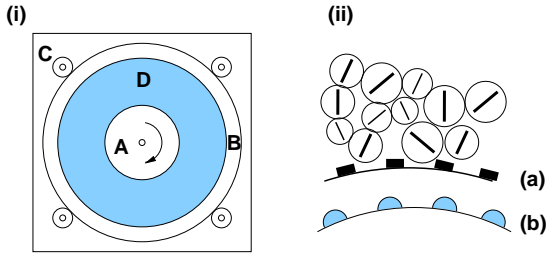


FIG. 1: (i) schematic top view of the experimental setup. (ii) schematic drawing of the disks close to the shearing wheel. (a) experimental realization of the walls. (b) realization of the walls in the simulation.

mean azimuthal velocity decreases roughly exponentially with distance from the inner shearing wheel, and within the statistical fluctuations, there is shear rate invariance. The mean particle spin oscillates around zero as the distance, $r - R$ from the wheel increases, but falls rapidly to zero away from the shearing surface. The distributions for the tangential velocity and the particle spin show a complex shape particularly for the grain layer nearest to the shearing surface, indicating a complicated dynamics, where velocity distributions near the inner wheel are very wide and non-Gaussian.

A. Simulations

There are a variety of numerical studies involving shearing. Some of these focus on stress-strain relations [24, 25, 26, 27, 28, 29, 30, 31, 32, 33], and others deal with shear banding in specific geometries [24, 25, 32, 33, 34, 35, 36, 37, 38]. In the present study, we present MD simulations and investigate the kinematic properties of a model system which was structured so that its realization is as close as possible to the physical system discussed here, a goal partially achieved already in [14, 39].

B. Overview of the paper

The rest of this paper is constructed as follows. The experimental set-up is reviewed in section II. The similarities and differences between the simulations and the physical system are discussed in section III. The initial conditions and the steady state are examined in section IV, and the results concerning velocity- and spin-distributions are presented in section V for different densities.

II. EXPERIMENTAL SETUP AND PROCEDURE

In this section we give enough details so that the reader can appreciate key aspects of the experiments and how the experiments relate to the simulations. The experimental setup and results are discussed in more detail in Refs. [14, 15, 16]. The apparatus, as sketched in Fig. 1, consists of (A) an inner shearing wheel (with radius R), and (B) an outer, stationary ring confined by (C) planetary gears. In the experiments, a bimodal distribution of disks (D) is used, with about 400 larger disks of diameter 0.899 cm, and about 2500 smaller disks of diameter 0.742 cm. An inhomogeneous distribution is useful, since it limits the formation of hexagonally ordered regions over large scales, even though there might still allow some short range order [40]. We use the diameter, $d = d_{\text{small}}$, of the smaller disks as a characteristic length scale throughout this study.

The experimental walls are fixed, corresponding to a *constant volume boundary condition*. All particles are inserted into the system and the shear is applied via the inner wall for several rotations, before averages in the nominally steady state are taken. If not explicitly mentioned, averages in the simulations are performed after about three rotations starting at $t = 180$ s, and extending over three rotations, until $t = 360$ s.

The mean packing fraction $\bar{\nu}$ (fractional area occupied by disks) is varied in the experiment over the range $0.789 \leq \bar{\nu} \leq 0.828$. As we vary $\bar{\nu}$ we maintain the ratio of small to large grains fixed, modulo small variations due to the fact that particle numbers can only be adjusted by integer jumps. Note that the effect of the wall particles for the calculation of the global packing fraction is very small. For computing the packing fraction in the simulations, only half the volume of the small particles glued to the side walls is counted, so that these boundary particles always contribute $\bar{\nu}_{\text{wall}} = 0.0047$ to $\bar{\nu}$.

An important question is how the system response depends on the shearing rate, which is set by Ω , the rotation rate of the inner wheel. A variation of Ω over $0.0029 \text{ s}^{-1} \leq \Omega \leq 0.09 \text{ s}^{-1}$ in the experiments shows rate independence in the kinematic quantities, except for some small, apparently non-systematic variations with Ω . A few simulations with $0.01 \text{ s}^{-1} \leq \Omega \leq 1.0 \text{ s}^{-1}$ showed clear rate independence for the slower shearing rates $\Omega \leq 0.1 \text{ s}^{-1}$, although the situation is less clear at the higher end of these rates.

III. SIMULATION METHOD AND SIMILARITY TO THE EXPERIMENT

Details of the simulations have been presented elsewhere [32], and we will not repeat these. However, we note that the model is a soft-particle MD model. As noted, the parameters used in the model were chosen to match the experiments as reasonably as possible. Specif-

ically, the radii, static friction coefficient and density of the particles, and the size of the container match the experimental values. The boundary conditions are chosen to mimic those in the experiment, see Sec. II. However, the “teeth” used on the inner and outer ring of the experiment are replaced by small disks with diameter d_{wall} , see Fig. 1. The properties of the particles and the parameters for the (linear) force laws [32, 41] are summarized in Table I.

Property	Values
Diameter d_{small} , Mass m_{small}	7.42 mm, 0.275 g
Diameter d_{large} , Mass m_{large}	8.99 mm, 0.490 g
Wall-particle diameter d_{wall} ,	2.50 mm
System/disk-height h	6 mm
Normal spring constant k_n	352.1 N/m
Normal viscous coefficient γ_n	0.19 kg/s
Tangential viscous damping γ_t	0.15 kg/s
Coulomb friction coefficient μ	0.44
Bottom friction coefficient μ_b	2×10^{-5}
Material density ρ_0	1060 kg m^{-3}

TABLE I: Microscopic material parameters of the model.

As in the experiment, several packing fractions of the shear-cell are investigated in the simulations (see Table II). For too low density, in the *sub-critical* regime, the particles are pushed away from the inner wall and lose contact, so that shearing stops. For too high densities, dilation and thus shear are hindered and the system becomes *blocked*. The intermediate regime $0.793 \leq \bar{\nu} \leq 0.809$ is of major interest in this study. Note that the range of densities that allow for the steady state shear flow is extremely narrow. However, we remark that the transition points between the three regimes quantitatively agree between experiments and simulations.

Still, there remain some nominally modest differences between the experiment and the simulation, which may lead to differences between results for the two realizations. The main differences are:

- The numerical code used here accounts for a very weak friction with the bottom plate only, presumably smaller than reality and thus allowing less damping of the particles. In addition, the reduced friction in the experiment is achieved by powder on the bottom plate and this may lead to somewhat inhomogeneous friction between the substrate and particles.
- Related to the bottom friction is a possible small tilt of the real particles out of plane of observation, connected to increased tangential and frictional forces due to increased, artificial, normal forces.
- The particle-wall (and also the particle-particle) contacts are modeled by simple linear force laws

Global Volume Fraction $\bar{\nu}$	Number of Particles		Flow Behavior
	small	large	
0.789	2462	404	sub-critical
0.791	2469	405	
0.793	2476	406	
0.796	2483	407	
0.798	2490	408	
0.800	2498	409	
0.800	2511	400	
0.802	2520	399	
0.804	2511	410	
0.805	2524	404	shear flow
0.807	2518	412	
0.807	2545	394	
0.809	2525	414	_____
0.810	2538	407	
0.811	2555	399	_____
0.819	2560	418	
0.828	2588	422	

TABLE II: Details of the simulation runs provided in this study. Mentioned are those particle numbers for which data were available in both experiment and simulation. The horizontal lines in the last column mark the transition between the sub-critical (the blocked) range of density with the shear flow regime.

and thus, possibly, do not reproduce reality to the extent desired. More complicated non-linear or hysteretic or plastic models [28, 29, 30, 31, 42, 43, 44] are far from the scope of this study.

- In the original experiment there existed a small bump on the inner wheel (a deviation from the ring-shape, which in the end leads to a slightly larger effective radius of the inner wall. A larger radius has the strongest effect in the case of low volume fractions, where the particles are easily moved away from the inner wheel.
- There is also a difference between the way the initial state is prepared for the experiments and the simulations. The starting state in the experiments is a nearly uniform density at the mean packing fraction, $\bar{\nu}$. The initial state of the simulation is an initially dilated state, which is then compressed. This preparation method is described below.

These factors apply for all the comparisons between the simulation- and experimental data to follow. While there are differences in various details, many qualitative and quantitative results are in agreement for the experiment and simulation.

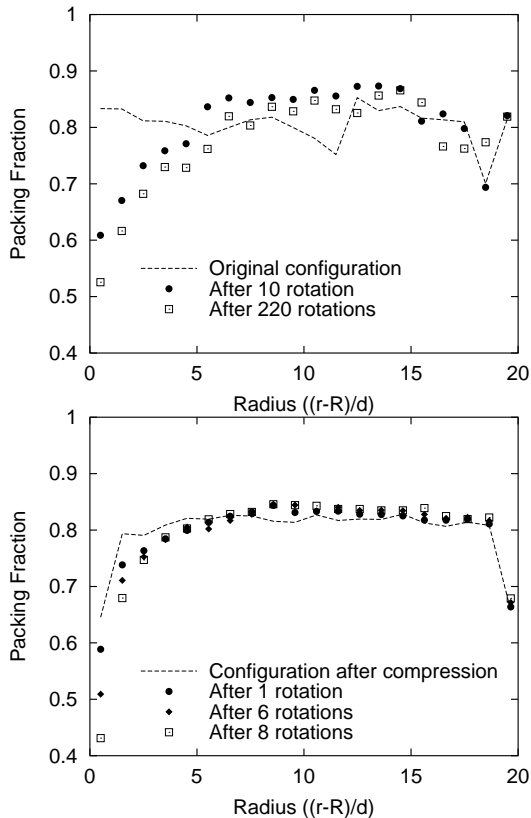


FIG. 2: Evolution of the packing fraction ν for different times versus radial distance $(r - R)/d$ from the wheel in units of disk diameters. The upper panel shows experimental data, the lower one simulation results.

IV. INITIAL CONDITIONS AND STEADY STATE

In this section, we explore the initial evolution of the system to a nominally stationary state, characterized by a dilated region near the shearing wheel, with large fluctuations in local density and velocity. Before collecting the data in the experiment, the inner wheel ran typically for 60 min at the highest shearing rate, corresponding to at least 20 rotations of the inner wheel. In the simulation, however, the preparation had to be limited in order to reduce the comparatively long computation time. The simulations are prepared for about three rotation periods, because a few runs with preparation times of up to ten periods of rotation did *not* show further relaxation effects. However, the much longer relaxation time of tens to hundreds of periods as used in the experiment was not reached, so that long time relaxation effects cannot be ruled out for the simulations presented here.

A. Preparation Procedure

As noted, the preparation procedure of the simulations is a dilute state. Specifically, the system starts with an

extended outer ring $R_{\text{prepare}} > R_o = 25.24$ cm. While the outer ring is expanded, the inner ring starts to rotate (counterclockwise) with constant angular velocity $\Omega = 0.1 \text{ s}^{-1}$. The radius of the outer ring is then reduced within about two seconds to reach its desired value R_o . Afterwards, the outer ring is kept fixed and the inner ring continues to rotate until at $t = t_{\text{max}}$ the simulation ends. Due to the constant volume in the experiment, the disks are inserted one by one until the desired number and density are reached. This difference, which can be seen in Fig. 2, affects the initial density, but should not influence results for the steady state.

B. Time-evolution of density profiles

The procedures for establishing a steady state were necessary because an initial, homogeneous density becomes radially non-uniform as a consequence of shear-induced dilatancy, for both experiment and simulation. Starting from a fairly uniform random packing (dashed lines in Fig. 2, for $\bar{\nu} = 0.804$), a dilated region forms close to the sheared inner wheel. There are minimal changes in the density after about 5 rotations of the inner wheel. Given a CPU-time of 1-2 days per rotation, we did not extend simulations over more than ten rotations, so that the true long-time behavior may not be captured here. Particle rearrangements have been observed over much longer relaxation times experimentally [16].

When making comparisons between the model and the experiment, it is important to keep in mind the following differences in obtaining local density data:

- Fill-up procedure (Section IV A). The dashed line from the simulations in Fig. 2 is obtained after a few seconds of compression *and* shear, so that a transient state between the initial and the steady state of the shear band is visible. The experimental data are obtained from the static initial state, where no onset of the shear band could take place.
- Averaging Procedures. The simulation data are averaged over full rings around the symmetry center of the shear-cell, whereas in the experimental system only radial slices that correspond to one quarter of the entire apparatus were observed. Even though averages were computed over an extended time interval, a systematic error due to this procedure cannot be ruled out. Because of possible circumferential fluctuations associated with this averaging process, the area under the experimental curves is not necessarily constant, nor necessarily identical to the global density.
- Experimental density determination. In the experiment the local density is measured via optical intensity methods, where there is some uncertainty due to light scattering and non-linear transmission.

Due to these possible systematic differences between the local densities obtained from experiment and from simulation, we take the freedom to adjust the local density data, as described below, when making comparisons between simulations and experiments.

C. Density difference between experiment and simulation

The method used to measure the local packing fraction in the experiment involves a calibration with some uncertainty, in addition to the fact that the real particles are not perfect disks as assumed in the simulation. Specifically, data are obtained by using the fact that UV light is strongly attenuated on passing through the photoelastic disks. This technique is calibrated against packings with well known area fractions, such as square and hexagonal lattices. There are still some small systematic uncertainties in this procedure, and if one computes the packing fraction using the data given in the upper part of Figure 2, a packing fraction higher than the global one is found. For that reason, in Fig. 3, we shift the experimental local density data downward by a constant value of $\nu_{\text{shift}} = 0.08$.

V. CHANGING THE PACKING FRACTION

In this section, the dependence of the local density, the forces, and the kinematics of the system are examined as a function of $\bar{\nu}$, the mean packing fraction. Using this global density $\bar{\nu}$ as a parameter has led to the discovery of a novel transition as the system approaches a critical packing fraction, $\bar{\nu}_c$ [15]. In the experiment we found $\bar{\nu}_c \sim 0.792$ versus $\bar{\nu}_c \sim 0.793$ in the simulations.

The reason for this $\bar{\nu}$ -dependence is easy to understand by imagining what would happen if $\bar{\nu}$ were very low. In this case, grains would easily be pushed away from the wheel, and after some rearrangements they would remain at rest without further contact with the moving wall. Increasing $\bar{\nu}$ by adding more and more grains would lead to the critical mean density, $\bar{\nu}_c$, such that there would always be at least some grains subject to compressive and shear forces from the boundaries. By adding more grains, the system would strengthen, more force chains would occur, and grains would be dragged more frequently by the shearing wheel. If even more particles were added, the system would become very stiff and eventually would become blocked, i.e. so dense that hardly any shearing can take place. In the extreme limit, due to large compressive forces and deformations, permanent plastic deformations might occur and brittle materials even might fracture. However, due to the large deformations possible with polymeric material used in the experiment and due to the relatively weak forces applied, none of these effects is evidenced.

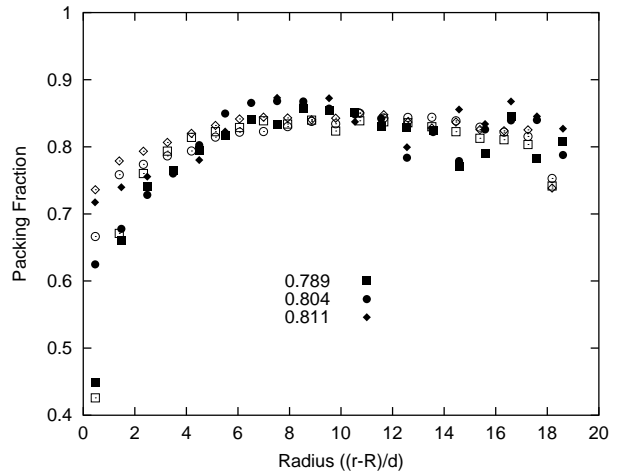


FIG. 3: Volume fraction ν , plotted against the dimensionless distance from the origin $(r - R)/d$, for different initial global densities $\bar{\nu}$ (not shifted). The open symbols give simulation data with $\bar{\nu}$ as given in the inset. The solid symbols show experimental data $\nu - \nu_{\text{shift}}$, with $\nu_{\text{shift}} = 0.08$.

A. Density

We first consider the local density profiles. In Fig. 3, we show ν vs. $(r - R)/d$ for several $\bar{\nu}$ values for both experiment and simulation. The data show good quantitative agreement within the fluctuations between experiment and simulation (after the systematic shift-correction explained above in subsection IV C). There is a clear difference in density between the dynamic, dilute shear zone and the static outer area. From the density data, we infer a width of the shear zone of about 5-6 particle diameters – from both experiment and simulation.

B. Velocity and spin profiles

In this subsection, we focus on the change in the velocity and spin profiles with changing $\bar{\nu}$. In Fig. 4, we show data for the velocity profiles for different $\bar{\nu}$ from both the experiment and the simulation. The profiles for the normalized velocity, $v_\theta/(\Omega R)$, show a roughly *exponential decay*, although there is some clear curvature in the experimental data at the outer edge of the shear zone, where the saturation level is reached. This *saturation level* of fluctuations in the velocity is at a higher level in the simulations, possibly due to the systematically larger shear rate in simulations used to save CPU-time, or due to the model for bottom friction. However, the logarithmic scaling over-amplifies this very small difference.

In the experiment, the amplitude of the exponential term (the velocity of the particles close to the inner wall, v_0) decays steadily to zero as $\bar{\nu}$ decreases towards $\bar{\nu}_c$. The simulation data show a weaker decay of the velocity at the inner wall with decreasing density. The fact that $v_0/(\Omega R) \ll 1$ indicates that as $\nu \rightarrow \nu_c$, either slip

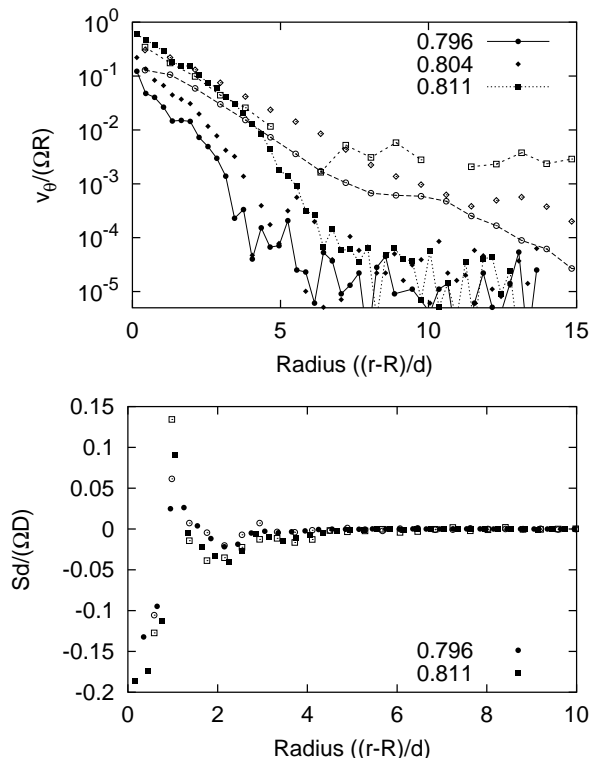


FIG. 4: Velocity and spin profiles for selected packing fractions $\bar{\nu}$. The solid and open symbols denote experimental and simulation data, respectively.

or intermittent shear takes place at the inner wall. Only values of $v_0/(\Omega R) = 1$ would correspond to perfect shear in the sense that the particles are moving with the wall without slip. For high densities, the agreement between experiments and simulations is reasonable, but for low densities, the magnitude of the velocities differs strongly. This may be due to either the differences in bottom- or wall-friction, or due to more irregular and differently shaped walls in the experiments, causing more intermittency and thus reduced mean velocities.

The experimental and the simulated profiles for the scaled particle spin, $Sd/(\Omega D)$, evolve in a similar manner with $\bar{\nu}$. Oscillations from negative to positive and back to negative spins are obtained, indicating at least partial rolling of the layers adjacent to the inner wall [45]. The mean spins are a little higher for all the simulations than in the experiment, possibly due to differences in the bottom friction or due to differences in the shearing surfaces.

The agreement in the velocity profiles is at least promising, given that the bottom friction may be wrong by a substantial amount. Especially for higher densities there is good quantitative agreement. Indeed, it is for this case that the bottom friction and wall effects are expected to be least important, since in this regime, the particle-particle interaction forces are at their strongest, and intermittent behavior is much relatively unlikely.

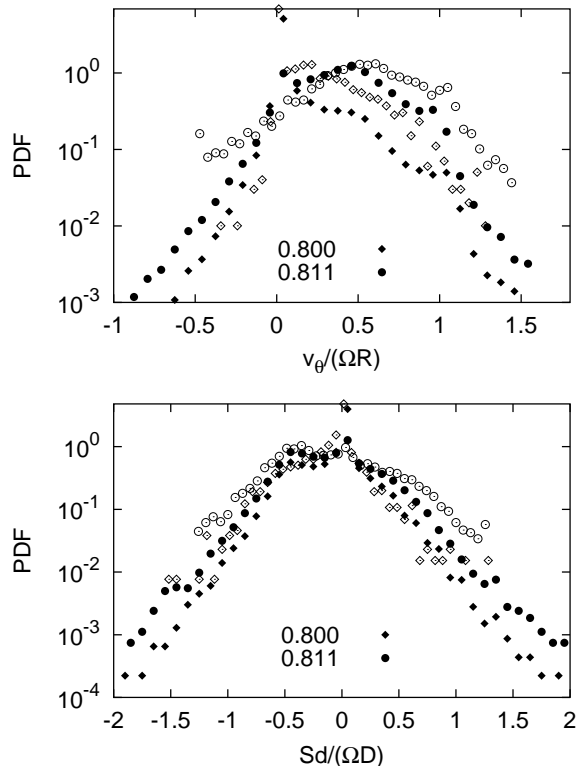


FIG. 5: Velocity and spin distributions close to the inner wall. The solid symbols denote experimental, the open symbols simulation data.

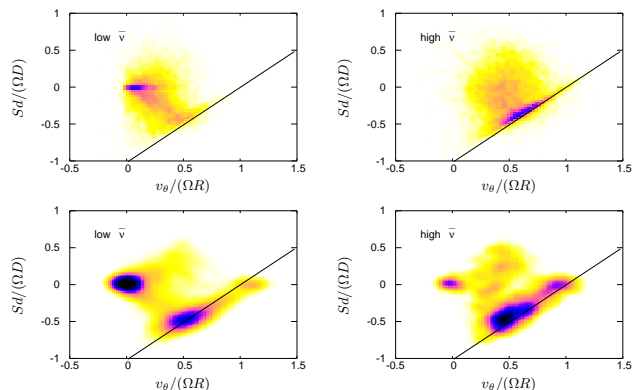


FIG. 6: 2D probability density for $v_\theta/(\Omega R)$ and $Sd/(\Omega D)$ for $0 < (r - R)/d < 1$. Darker regions correspond to higher probability densities. The upper and lower panels correspond to simulation and experimental data, respectively.

C. Velocity Distributions

From the previous section, we infer that changing the packing fraction affects not only the profiles, but also the distributions of the velocity. In Fig. 5, we show the velocity distributions in a one-particle wide radial bin next to the inner wheel for various $\bar{\nu}$ -values from the experiment and the simulation.

The data clearly show that the peaks near the origin, corresponding to non-rotating particles at rest, become weaker with increasing density. Furthermore, the regions with negative spin and nonzero v_θ grow with increasing $\bar{\nu}$. The fact that increasing $\bar{\nu}$ leads to a decreasing number of stationary particles is not surprising. But the formation of the second peak in the velocity distribution at $v_\theta/(\Omega R) \simeq 0.5$ is not as intuitive as the small peak at unity.

A key to understanding this phenomenon is contained in the two-variable distribution $P(v_\theta/(\Omega R), Sd/(\Omega D))$, as shown in Fig. 6 for high (right) and low (left) density $\bar{\nu}$. The upper data are experimental and the lower data are from simulations. The probability is coded in grayscale with dark denoting higher probabilities. This figure indicates two distinct features, corresponding to two qualitatively different processes. The first feature is the concentration of probability around $(0, 0)$, which corresponds to a state where the disks are essentially at rest, without spin or translation. The other feature is a concentration of probability around the line $v_\theta/(\Omega R) = 1 + Sd/(\Omega D)$, which corresponds to non-slip motion of grains relative to the wheel. No-slip here means, that the particles execute a combination of backwards rolling and translation, such that the wheel surface and the disk surface remain in continuous contact. Thus, the peak at $v_\theta/(\Omega R) = 0$, which is strong for low $\bar{\nu}$, corresponds to particles that are so weakly compressed that they can easily slip with respect to the shearing wheel. With higher density, and hence greater force at the contacts between the particles and the shearing wheel, slipping becomes less likely and the combination of translation and backwards rolling is the preferred state.

VI. SUMMARY

We have reported parallel experimental studies and Molecular Dynamics simulations of shearing in a two-dimensional Couette geometry. Here, an important goal was to benchmark such simulations in a setting where it was possible to have good overlap between the parameters relevant to the simulations and the experiments. In most respects, the numerical results are in good qualitative, and for some quantities good quantitative agreement with the experimental results [46].

Both simulations and experiments show rate-independence within the statistical errors, and the range of rates that were studied. We have particularly focused on the dependence of the shearing states on the global packing fraction. Good agreement between simulation and experiment was found for the density profiles associated with the formation of a shear band next to the inner shearing wheel with a characteristic width of about 5 to 6 particle diameters.

Both simulation and experiment also showed a roughly

exponential velocity profile. However, the simulations did not capture the density dependence of the experimental velocity profiles, nor some details of the shape, especially at the outer edge of the shear band. In this regard, further exploration of the role played by roughness of the shearing surface and the effect of the particle-bottom friction are necessary. The former can lead to more intermittent behavior, whereas the latter might explain the velocity-drop at the outer edge of the experimental shear band.

The alternating spin profiles in experiment and simulation agreed nicely, indicating a rolling of the innermost particle layers (parallel to the walls) over each other. Outside of the shear band, rotations are *not* activated, however. From the velocity- and spin-probability densities, a combination of rolling and sliding with the inner wall is evidenced. As the density decreases towards ν_c , increasingly more particles remain at rest – stopped by the bottom friction. With increasing density, more and more particles are dragged with the moving wall, but at the same time roll over each other – in layers, with strongly decreasing amplitude as distance from the moving wall increases.

VII. CONCLUSION AND OUTLOOK

The present study is of particular interest because of the intensive attempt to match as many of the detailed properties of the experiment as feasible by the corresponding properties in the simulation. Specifically, most of the parameters used in the simulation are fixed by experimental measurement. Nevertheless, certain properties of the system were sufficiently complex or difficult to determine exactly, so that there were some differences between the experimental and simulational realizations. In this category of complex properties are friction with the bottom surface, and the fact that the particles were not perfectly uniform. In spite of these differences, all the features seen in the experiment were also realized in the simulation. In many cases, the correspondence between simulation and experiment were quantitatively correct to within a few percent. In other cases, the simulation could be shifted appropriately so that agreement with the experiment was possible. Given the uncertainty in experimental parameters and/or small irregularities, this level of agreement is quite reasonable. The clear conclusion is that with sufficient care, MD modeling of a granular system can produce and predict experimental behavior, with the understanding that absolute quantitative agreement may be limited. Inevitably, in any experiment, small variabilities between particles or boundaries come into play at a sufficient level of detail. At this level agreement between simulation and experiment, and even between similar but distinct experiments must limit absolute agreement.

-
- [1] O. Reynolds, *Philos. Mag. Ser. 5* **50-20**, 469 (1885).
- [2] R. A. Bagnold, *Proc. Royal Soc. London* **225**, 49 (1954).
- [3] J. B. Knight, *Phys. Rev. E* **55**, 6016 (1997).
- [4] T. G. Drake, *J. of Geophysical Research* **95**, 8681 (1990).
- [5] R. M. Nedderman and C. Laohakul, *Powder Technol.* **25**, 91 (1980).
- [6] S. B. Savage and K. Hutter, *J. Fluid Mech.* **199**, 177 (1989).
- [7] O. Pouliquen and R. Gutfraind, *Phys. Rev. E* **53**, 552 (1996).
- [8] H. J. Herrmann, *Physikalische Blätter* **51**, 1083 (1995).
- [9] L. Vanel, P. Claudin, J.-P. Bouchaud, M. E. Cates, E. Clément, and J. P. Wittmer, *Phys. Rev. Lett.* **84**, 1439 (2000).
- [10] J. Geng, D. Howell, E. Longhi, R. P. Behringer, G. Reydellet, L. Vanel, E. Clément, and S. Luding, *Phys. Rev. Lett.* **87**, 035506 (2001).
- [11] J. Geng, R. P. Behringer, G. Reydellet, E. Clément, and S. Luding (2002), to be published.
- [12] C. T. Veje, D. W. Howell, and R. P. Behringer, *Phys. Rev. E* **59**, 739 (1999).
- [13] B. Miller, C. O'Hern, and R. P. Behringer, *Phys. Rev. Lett.* **77**, 3110 (1996).
- [14] C. T. Veje, D. W. Howell, R. P. Behringer, S. Schöllmann, S. Luding, and H. J. Herrmann, in *Physics of Dry Granular Media*, edited by H. J. Herrmann, J.-P. Hovi, and S. Luding (Kluwer Academic Publishers, Dordrecht, 1998), p. 237.
- [15] D. Howell, R. P. Behringer, and C. Veje, *Phys. Rev. Lett.* **82**, 5241 (1999).
- [16] D. W. Howell, R. P. Behringer, and C. T. Veje, *Chaos* **9**, 559 (1999).
- [17] D. W. Howell, Ph.D. thesis, Duke University, Department of Physics (1999).
- [18] E. Azanza, F. chevoir, and P. Moucheron, *J. Fluid Mech.* **400**, 199 (1999).
- [19] W. Losert, D. G. W. Cooper, and J. P. Gollub, *Phys. Rev. E* **59**, 5855 (1999).
- [20] H. Buggisch and G. Löffelmann, *Chemical Engineering and Processing* **26**, 193 (1989).
- [21] J. M. Rotter, J. M. F. G. Holst, J. Y. Ooi, and A. M. Sanad, *Phil. Trans. R. Soc. Lond. A* **356**, 2685 (1998).
- [22] J. M. F. G. Holst, J. Y. Ooi, J. M. Rotter, and G. H. Rong, *Journal of Engineering Mechanics ASCE* **125**, 94 (1999).
- [23] J. M. F. G. Holst, J. M. Rotter, J. Y. Ooi, and G. H. Rong, *Journal of Engineering Mechanics ASCE* **125**, 104 (1999).
- [24] S. Luding, M. Lätzel, and H. J. Herrmann, in *Handbook of Conveying and Handling of Particulate Solids*, edited by A. Levy and H. Kalman (Elsevier, Amsterdam, The Netherlands, 2001), pp. 39–44.
- [25] S. Luding, M. Lätzel, W. Volk, S. Diebels, and H. J. Herrmann, *Comp. Meth. Appl. Mech. Engng.* **191**, 21 (2001).
- [26] C. S. Campbell and C. E. Brennen, *J. Fluid. Mech.* **151**, 167 (1985).
- [27] D. J. Evans and G. P. Morriss, *Phys. Rev. Lett.* **51**, 1776 (1983).
- [28] O. R. Walton and R. L. Braun, *Acta Mechanica* **63**, 73 (1986).
- [29] C. Thornton and K. K. Yin, *Powder Technol.* **65**, 153 (1991).
- [30] C. Thornton, *Journal of Applied Mechanics* **64**, 383 (1997).
- [31] C. Thornton and S. J. Antony, *Powder Technology* **109**, 179 (2000).
- [32] M. Lätzel, S. Luding, and H. J. Herrmann, *Granular Matter* **2**, 123 (2000), cond-mat/0003180.
- [33] S. Masson, *J. Engineering Mechanics* **127**, 1007 (2001).
- [34] H.-J. Tillemans and H. J. Herrmann, *Physica A* **217**, 261 (1995).
- [35] C. Thornton and L. Zhang, in *Powders & Grains 2001*, edited by Y. Kishino (Balkema, Rotterdam, 2001), pp. 183–190.
- [36] M. Oda and K. Iwashita, *Int. J. of Engineering Science* **38**, 1713 (2000).
- [37] M. Oda and H. Kazama, *Géotechnique* **48**, 465 (1998).
- [38] F. Radjai, S. Roux, and J. J. Moreau, *Chaos* **9**, 544 (1999).
- [39] S. Schöllmann, *Phys. Rev. E* **59**, 889 (1999).
- [40] S. Luding, *Advances in Complex Systems* **4**, 379 (2002).
- [41] M. Lätzel, Master's thesis, Universität Stuttgart (1999).
- [42] O. R. Walton and R. L. Braun, *Journal of Rheology* **30**, 949 (1986).
- [43] R. W. Mei, H. Shang, O. R. Walton, and J. F. Klausner, *Powder Technology* **112**, 102 (2000).
- [44] C. Thornton, *Géotechnique* **50**, 43 (2000).
- [45] S. Luding, J. Duran, E. Clément, and J. Rajchenbach, *J. Phys. I France* **6**, 823 (1996).
- [46] This is astonishing when the possible discrepancies concerning particle shape and boundaries, as well as the partially huge differences between experimental reality and the particle-particle and particle-wall contact models in the simulation are considered